IFS #201

Three Dimensional Particle Simulation of Drift Wave Fluctuations in a Sheared Magnetic Field

R. D. Sydora, J. N. Leboeuf, D. R. Thayer,
P. H. Diamond and *T. Tajima*
Institute for Fusion Studies
The University of Texas at Austin
Austin, Texas 78712

Abstract

Three dimensional particle simulations of collisionless drift waves in sheared magnetic fields were performed in order to determine the nonlinear behavior of inverse electron resonance dynamics in the presence of thermal fluctuations. It is found that stochastic electron diffusion in the electron resonance overlap region can destabilize the drift wave eigenmodes. Numerical evaluations based on a nonlinear electron resonance broadening theory give predictions in accord with the frequency and growth rates found in the simulation of short wavelength modes $(k_y \rho_s \gtrsim 1)$.

Low frequency drift wave induced turbulence is conjectured to be one of the important mechanisms for anomalous transport in tokamaks. An ingredient necessary for a theoretical model of turbulent transport is an understanding of the instability mechanism. Consequently, the stability of electrostatic normal mode perturbations in an inhomogeneous, collisionless plasma embedded in a sheared magnetic field has been a subject of interest over the past decade.[1-5] Specifically, the effects of electron orbit stochasticity have been proposed as a significant consideration in determining drift wave stability.[6,7]

In this Letter, the stability of electrostatic collisionless drift waves in a sheared magnetic field is investigated using a three dimensional electrostatic particle simulation model. It is found that modification of the linear electron dynamics due to overlapping electrostatic islands in the vicinity of the mode rational surfaces $\left(k_{\|} = k'_{\|} x = 0\right)$ can affect the stability of the linear drift wave eigenmodes.

The simulations are carried out in slab geometry with the inhomogeneous density profile, $n(x) = n_0 \kappa L_x e^{-\kappa x} / \left(1 - e^{-\kappa L_x}\right)$, in the x-direction. The system length in the x-direction is L_x, n_0 is the average number density, and $L_n \left(\equiv 1/\kappa, \kappa = -n'(x)/n\right)$ is the density scale length. The y and z-directions are homogeneous and periodic. A normal mode expansion of the fields and charge density is employed in the z-direction.[8] The electron dynamics are treated in the guiding center approximation for motion across the magnetic field and exact parallel motion is retained along the field.[9] The ion motion evolves exactly, according to the Newton-Lorentz equation. The magnetic field is given by $\mathbf{B} = B_0 \left[\hat{z} + \hat{y}\left(x - x_0\right)/L_s\right]$, where x_0 defines the central position of the rational surfaces and L_s is the shear scale length. The value $x_0 = L_x/2$ is chosen and the rational surfaces are concentrated in the middle of the simulation domain. The boundary condition on the electrostatic potential is $\phi(0) = 0 = \phi\left(L_x\right)$ and the eigenmode parity is dominantly even with respect to the rational surfaces. The rational surface positions are located at $x_{mn} = x_o \pm \left(n/m\right)\left(L_s L_y / L_z\right)$, where $k_y = 2\pi m / L_y$ and $k_z = 2\pi n / L_z$. Typical simulation parameters used are: $L_x \times L_y \times L_z = 12\rho_s \times 6\rho_s \times 1200\rho_s$, $\tau = T_e/T_i = 1$, $m_i/m_e = 500$, $L_s/L_n = 14$, $L_n/\delta = 16$, $v_e/\omega_{pe}\delta = 2.6$, $\omega_{ce}/\omega_{pe} = 11$, $k_y\rho_s = 1.1m$, $n_0 = 16$ particles/cell, $\omega_{ci}\Delta t = 0.07$, $m = 0, \pm 1, \ldots, \pm 16$, $n = 0, \pm 1, \ldots, \pm 5$, and the finite particle size is given by $a_x = 1.5\delta$, $a_y = \delta$, and $a_z = 270\delta$. The parameter definitions

are $T_e = m_e v_e^2$, $\rho_s = \sqrt{\tau} v_i / \omega_{ci}$, $\omega_{ci} = eB/m_i c$, $\omega_{pe}^2 = 4\pi n_0 e^2/m$ and δ is the unit grid spacing.

The analysis and interpretation of the simulation results consists of two parts. First, particle orbits and diffusive electron behavior are investigated in detail. Second, the wave potential fluctuations are temporally and spatially analyzed in order to determine their stability.

Test electrons are continuously selected in the vicinity of the mode rational surfaces and the spatial diffusivity is obtained. To determine the Chirikov condition[10] for stochasticity at the simulation thermal level in the mode rational surface region, the island width is compared with the mode rational surface separation. In the neighborhood of the electron resonance, the island width is approximately $\Delta x_T/\rho_s \simeq (4/\rho_s)\left(L_s \left|\phi_{mn}\right| / B v_e\right)^{1/2}$. This value is $5\left(\left|e\phi_{mn}\right| / T_e\right)^{1/2}$ for the simulation parameters. A crude estimate of the rational surface spacing is given by $\Delta x_{mn}/\rho_s = \left(-L_y L_s/\rho_s L_z\right)(\Delta n/\Delta m) \simeq 0.21 n/[m(m+1)]$. From the fluctuation levels measured in the simulation, $10^{-3} \lesssim e\phi_{mn}/T_e \lesssim 10^{-1}$, the island overlap condition is well satisfied ($\Delta x_T > \Delta x_{mn}$) and the electron orbits are stochastic as demonstrated in Fig. 1.

The diffusion coefficient, D, for test particles may be measured by using $D = \lim_{t\to\infty} \sum_{i=1}^{N} (\Delta X_i)^2 / 2Nt$, where ΔX_i is the change in position of the guiding center for the ith particle at time t and where N is the number of test particles. The guiding center displacement of test electrons in the x-direction as a function of time, initially located in the range $5 \lesssim x/\rho_s \lesssim 7$, is illustrated in Fig. 2a. The value of the test particle diffusion coefficient $\left(D = 0.006 \rho_s^2 \omega_{ci}\right)$ is verified by two independent calculations. One estimate is based on the potential fluctuations measured in the simulation assuming that resonant diffusion dominates. Another estimate is made using the exponential divergence of neighboring orbits, where the relation between the parallel correlation length and diffusion coefficient is determined. It is evident from Fig. 2a that the diffusion coefficient decreases beyond $\omega_{ci} t = 132$. This indicates that the diffusion process is time-dependent and, as will be shown, is related to the saturation of the potential fluctuations.

Using a modification of the resonance broadening theory of Dupree,[11] Hirshman and Molvig[6] derived a renormalized kinetic equation to describe the behavior of electrons in a

strongly turbulent plasma in a sheared magnetic field. For the case of resonance overlap, stochastic particle orbit behavior resulted in a net effect of electron orbit diffusion transverse to the magnetic field. The electrons decorrelate from the drift wave resonances at a rate of $\omega_c = \left[\left(k'_{\|} v_e\right)^2 D\right]^{1/3}$, where $k'_{\|} = k_y / L_s$. It was also found that at short wavelengths $\left(k_y \rho_s \gtrsim 1\right)$ the linearly stable modes can be nonlinearly destabilized for $\omega_c \gtrsim \omega$, where ω is the linear drift wave eigenmode frequency.

The renormalized electron density response is coupled to the linear ion response through the quasineutrality condition. This gives an eigenmode equation for the perturbed potential,[6]

$$d^2 \hat{\phi} / d\tilde{x}^2 + Q\left(\tilde{x}\right) \hat{\phi} = 0, \tag{1}$$

$$Q\left(\tilde{x}\right) = \frac{\left[\left(1+\tau\right)\frac{\omega}{\omega_*} + \zeta_i Z\left(\zeta_i\right)\left(1+\tau\frac{\omega}{\omega_*}\right)\Gamma_0(b) + i\left(\frac{\omega}{\omega_*}-1\right)\frac{\omega}{\omega_c} I^{(0)}\right]}{\left\{\zeta_i Z\left(\zeta_i\right)\left(\frac{\omega}{\omega_*}+\frac{1}{\tau}\right)\left[\Gamma_0(b)-\Gamma_1(b)\right] + 3i\left(\frac{\omega}{\omega_*}-1\right)\frac{\omega}{\omega_c} x_c^2 I^{(2)}\right\}}. \tag{2}$$

Here, the diamagnetic drift frequency is $\omega_* = \omega_{ci}\left(k_y \rho_s\right)\left(\rho_s / L_n\right)$, the correlation length is $x_c = \left(\omega_c / \omega *\right)\left(L_s / L_n\right)\left(m_e / 2m_i\right)^{1/2}$, $\Gamma_n(b) = e^{-b} I_n(b)$, I_n are modified Bessel functions, $b = \left(k_y \rho_s\right)^2 / \tau$, $\zeta_i = \omega / \sqrt{2} k_{\|} v_i$, and $\tilde{x} = x / \rho_s$. The turbulently modified electron source term,

$$I^{(0)} = \int_0^\infty ds\, g, \tag{3}$$

and the mode broadening term,

$$I^{(2)} = \int_0^\infty ds\, s\left\{1 - 3s^3 h\left[1 - \left(x/x_c\right)^2 s^2 h/2\right]/4\right\} g, \tag{4}$$

change the basic linear eigenmode stability, where $g = h^{1/2} \exp\left[i\left(\omega/\omega_c\right) s - \left(x/x_c\right)^2 s^2 h/4\right]$, and $h = \left(1+s^3\right)^{-1}$. The electron response integrals are numerically evaluated and the eigenmode equation can be solved using a standard shooting method. To verify this approach, comparisons are made with an initial value code which follows the time evolution of the perturbed distribution function and electrostatic potential.[12] The eigenfunctions, $\hat{\phi}\left(\tilde{x}\right)$, and eigenvalues, $\omega = \omega_r + i\gamma$, are determined by varying the parameters $k_y \rho_s$, τ, L_s / L_n, m_i / m_e, and ω_c / ω_*, where ω_c / ω_* measures the strength of the background fluctuations causing the diffusion in x. In Fig. 2b, the growth

rate is represented as a function of the decorrelation rate for various wave numbers. The solid circles correspond to the predicted growth rates at the measured simulation decorrelation rate.

Figure 3 shows the time history of the electrostatic energy for the single and multiple rational surface cases. For the multiple rational surface case with $k_y\rho_s \geq 1$, there is approximately a 30 percent increase in the amplitude above the thermal fluctuation level and it occurs over several drift periods. Total energy conservation was less than half a percent over the entire length of the run. The growth rates of the fluctuations correspond closely to the predictions derived from the nonlinear eigenmode equation. The variation of the mode in the x-direction agrees qualitatively with the wave function obtained from the eigenmode equation. The growth rates and real frequencies for various mode numbers, as well as comparisons with the analytic model are shown in Fig. 4.

The enhanced fluctuation level is large enough to cause relaxation of the equilibrium density profile in the resonance overlap region. The decrease in the electron diffusion coefficient illustrated in Fig. 2 coincides with the saturation time of the longest wavelength modes, $(m,n) = (\pm 1, n)$. The increased amplitude of the potential fluctuations is sufficient to push particles out of the resonance overlap region. This changes the diffusivity of the particles, which in turn affects the mode stability. The enhanced diffusion out of the resonance overlap region manifests itself as a local density profile relaxation. Employing a more exact analysis of the two time diffusion orbit integrals, the time dependence of the diffusion coefficient is predicted for a system with a finite width resonance region.[13] The time for an electron to diffusively pass through the finite resonance region roughly corresponds to the initial departure of the diffusion coefficient from time independence.

For the previous parameters, the entire wave number spectrum ($k_y\rho_s$) gave positive growth rates. We also consider the situation where additional stable, long wavelength modes ($k_y\rho_s < 1$) are present in the simulation. The parameters outlined previously were used with the following alterations: $\omega_{ce}/\omega_{pe} = 35$, $k_y\rho_s = 0.31m$, and $\omega_{ci}\Delta t = 0.14$. Due to computational limitations this is the largest system that could be used.

The fluctuation level of the electrostatic energy remains at the thermal level for the entire length of the simulation as is illustrated in Fig. 3a. No observable changes in the

equilibrium density profile occurred. Particle orbit measurements verify that the electrons are stochastic and resonance overlap is well satisfied. Growth for the modes with $k_y\rho_s \gtrsim 1$ was not observed. One possible discrepancy between simulation and theory arises from the addition of large amplitude, damped, long wavelength fluctuations. Through mode coupling, these modes can provide a sink of energy for the more unstable, short wavelength fluctuations. Another possible influence on the eigenmode stability is nonlinear ion Landau damping effects (i.e., ion Compton scattering).[14] The Compton scattering process causes a transfer of mode spectrum energy to long wavelengths while producing additional damping to short wavelengths.

We have performed approximate calculations for the damping effects of mode coupling and ion Compton scattering on the modes with $k_y\rho_s \gtrsim 1$. For typical triplet interactions in this sheared configuration, strong local coupling of the large amplitude long wavelength stable modes is on the order of the stochastic growth rate. Also, the nonlinear Landau damping rate is found to be lower than the linear shear damping rate by roughly a factor of three. Consequently, the stable results found for the simulation which included large amplitude, long wavelength modes can be explained theoretically by including mode coupling damping effects on the short wavelength modes.

In conclusion, we have performed three dimensional particle simulations with conditions in which a nonlinear destabilization mechanism for drift waves is operative. It should be noted that this work is subject to the computer capabilities at the time of computation so that effects may have been neglected which could give rise to the enhanced fluctuations.

Acknowledgements

The authors wish to thank C. O. Beasley, R. H. Berman, W. W. Lee, K. Molvig, M. N. Rosenbluth and P. W. Terry for many helpful discussions and criticisms. This work was supported by the U. S. Department of Energy under Contract No. DE-FG05-80-ET-53088 and the National Science Foundation under Grant No. ATM-82-14730.

References

1. L. D. Pearlstein and H. L. Berk, Phys. Rev. Lett. **28**, 220 (1969).
2. D. W. Ross and S. M. Mahajan, Phys. Rev. Lett. **40**, 324 (1978).
3. K. T. Tsang, P. J. Catto, J. C. Whitson and J. Smith, Phys. Rev. Lett. **40**, 327 (1978).
4. W. W. Lee, W. M. Nevins, H. Okuda and R. B. White, Phys. Rev. Lett. **43**, 347 (1979).
5. R. D. Sydora, J. N. Leboeuf, and T. Tajima, Phys. Fluids **28**, 528 (1985).
6. S. P. Hirshman and K. Molvig, Phys. Rev. Lett. **42**, 648 (1979).
7. C. F. Zhang, R. Marchand and Y. C. Lee, Phys. Fluids **25**, 2264 (1982).
8. C. Z. Cheng and H. Okuda, J. Comp. Phys. **25**, 133 (1977).
9. W. W. Lee and H. Okuda, J. Comp. Phys. **26**, 139 (1978).
10. G. M. Zaslavskii and B. V. Chirikov, Sov. Phys. Uspekhi **14**, 549 (1972).
11. T. H. Dupree, Phys. Fluids **10**, 1049 (1967).
12. C. O. Beasley, K. Molvig and W. I. van Rij, Phys. Fluids **26**, 678 (1983).
13. A. Salat, Z. Naturforsch. Teil A **38**, (1983).
14. P. H. Diamond and M. N. Rosenbluth, Institute for Fusion Studies Rep. No. IFSR-24 (1981).

Figure Captions

Fig. 1 Test electron orbits in $(x - v_{\|})$ space as a function of time. Open circles refer to initial particle positions and solid circles are rational surface positions for mode (m, n).

Fig. 2 (a) Guiding center displacement of test electrons in the x-direction as a function of time. (b) Theoretical growth rate as a function of the decorrelation rate for various wavenumbers. Solid circles are predicted growth rates using measured simulation values of the decorrelation rate.

Fig. 3 Time history of the total electrostatic energy for (a) multiple rational surface case and (b) single rational surface. The arrow indicates electrostatic energy level necessary to satisfy the island overlap.

Fig. 4 Theoretical and measured simulation growth rates and real frequencies for various wavenumbers.

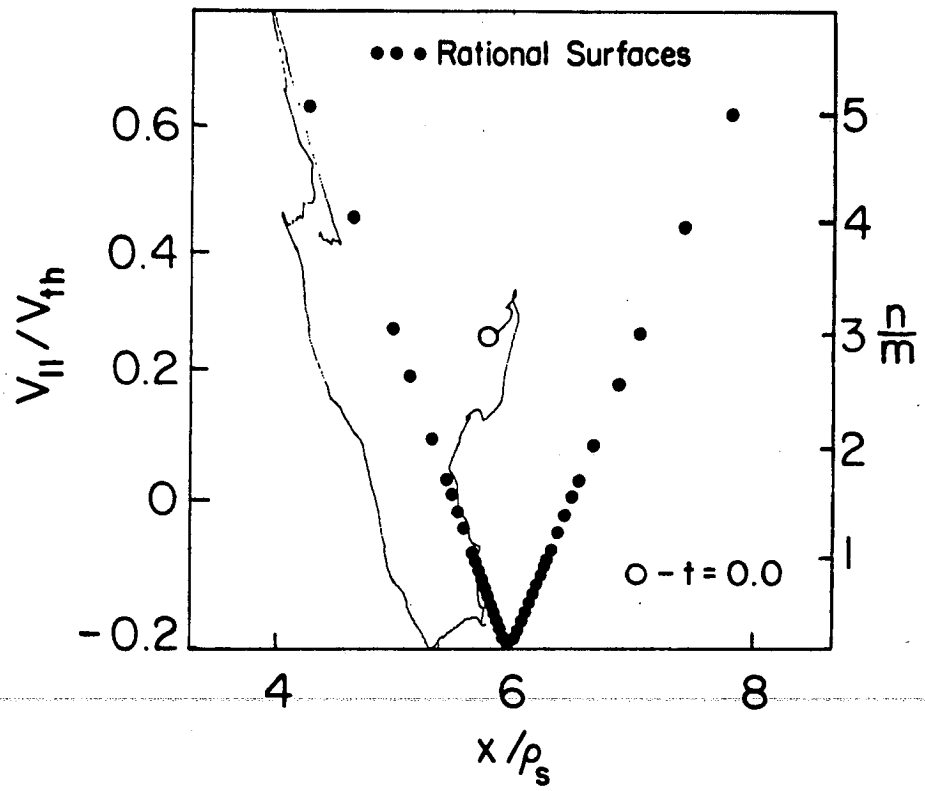
••• Rational Surfaces
0.6
0.4
0.2
0
-0.2
$V_{||}/V_{th}$
5
4
3 n/m
2
1
o - t = 0.0
4
6
8
x/ρs

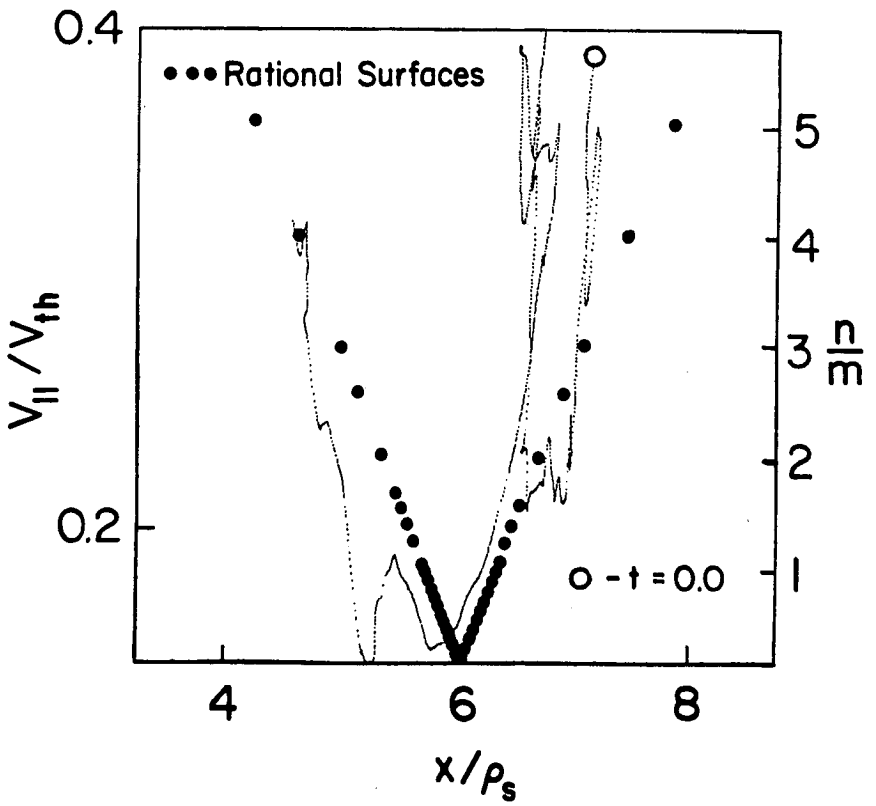
0.4
••• Rational Surfaces
0.2
$V_{||}/V_{th}$
5
4
3 n/m
2
1
o - t = 0.0
4
6
8
x/ρs

FIG. 1

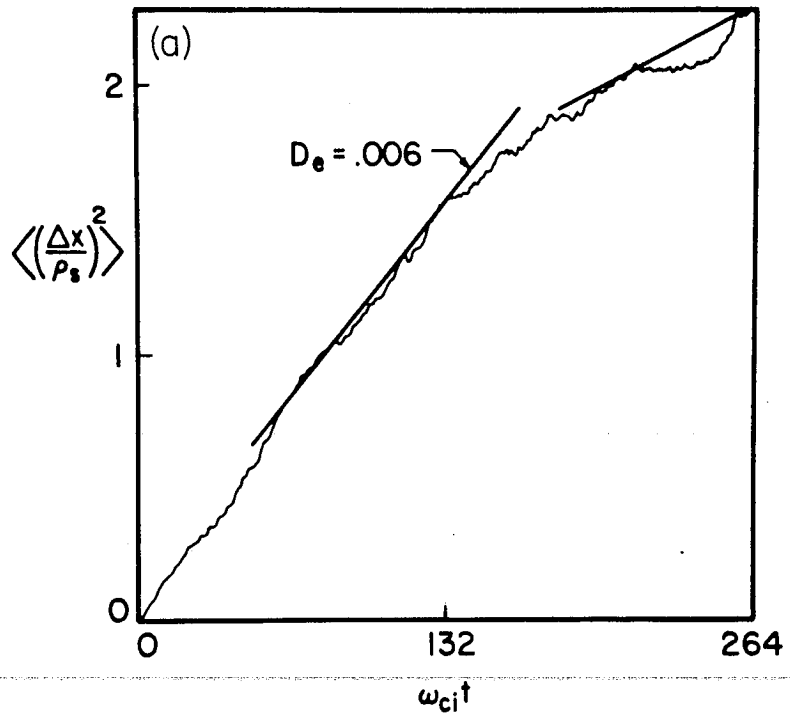
(a)
$D_e = .006$
$\left\langle \left(\frac{\Delta x}{\rho_s}\right)^2 \right\rangle$
2
1
0
0
132
264
$\omega_{ci} t$

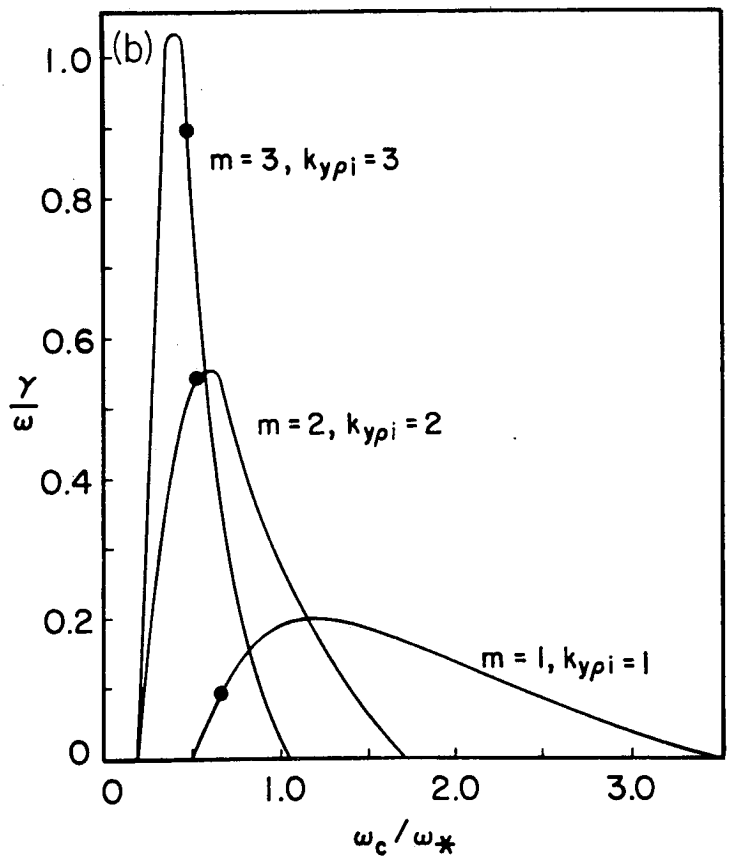
(b)
$m = 3,\ k_{y\rho i} = 3$
$m = 2,\ k_{y\rho i} = 2$
$m = 1,\ k_{y\rho i} = 1$
$\frac{\gamma}{\omega}$
1.0
0.8
0.6
0.4
0.2
0
0
1.0
2.0
3.0
ω_c / ω_*

FIG. 2

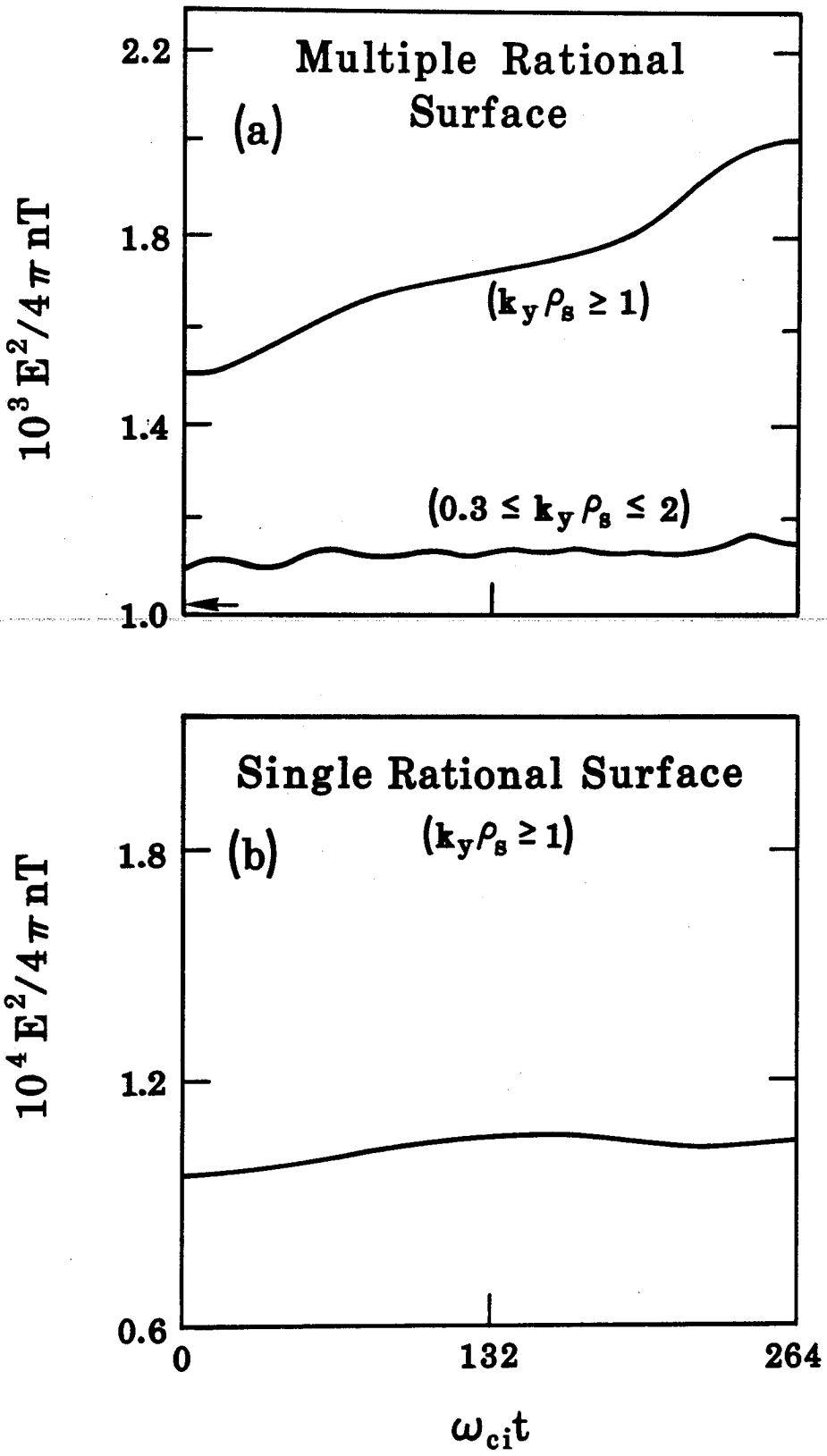
Multiple Rational Surface
(a)
$(k_y \rho_s \geq 1)$
$(0.3 \leq k_y \rho_s \leq 2)$
$10^3 E^2/4\pi nT$
2.2
1.8
1.4
1.0
Single Rational Surface
$(k_y \rho_s \geq 1)$
(b)
$10^4 E^2/4\pi nT$
1.8
1.2
0.6
0
132
264
$\omega_{ci} t$

FIG. 3

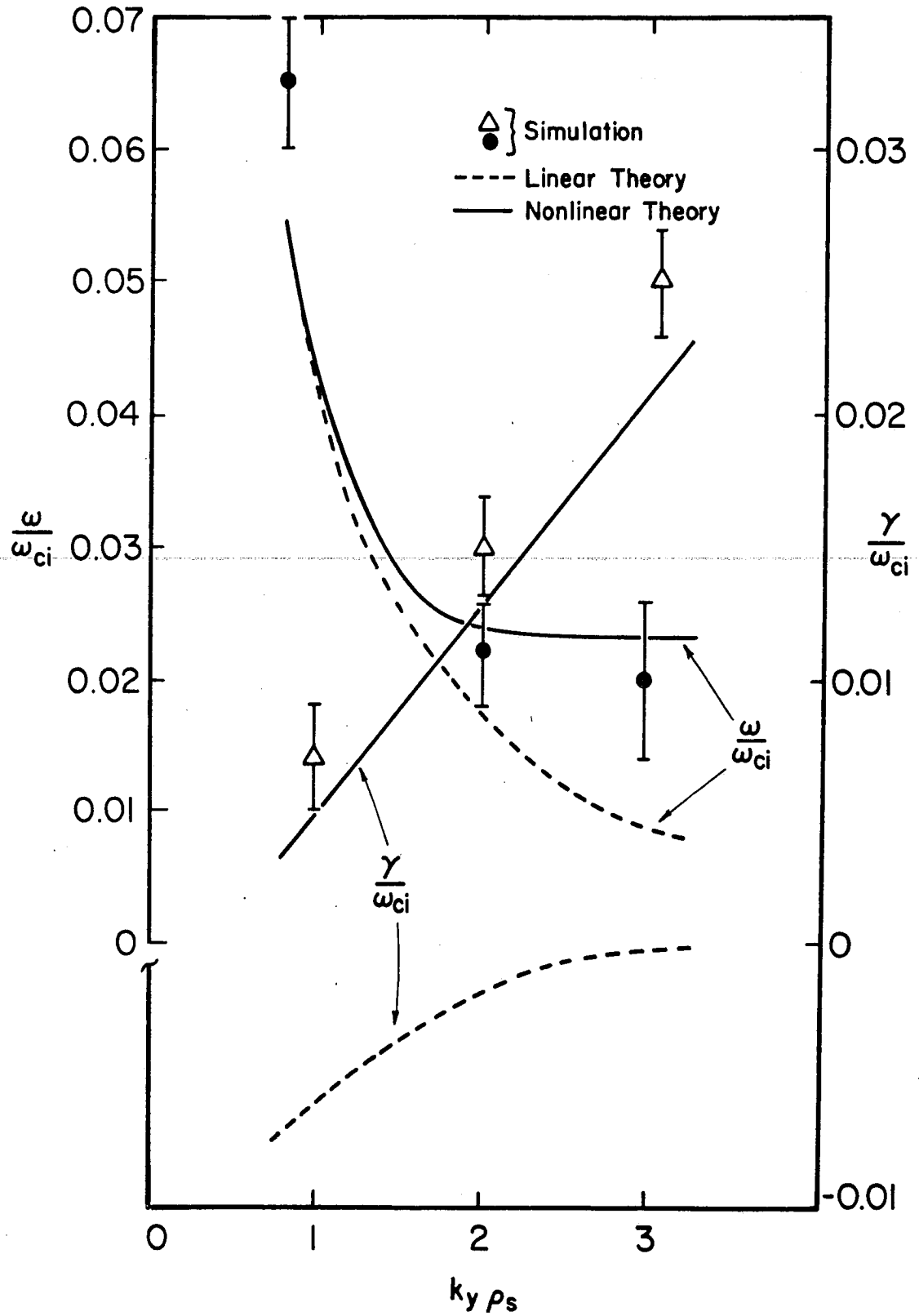
0.07
0.06
0.05
0.04
0.03
0.02
0.01
0
0.03
0.02
0.01
0
-0.01
Simulation
Linear Theory
Nonlinear Theory
ω/ωci
γ/ωci
ω/ωci
γ/ωci
0
1
2
3
ky ρs

FIG. 4